Energy-Yielding Mini Heat Thermocells with WS₂ Water-Splitting Dual System to Recycle Wasted Heat

Yi-Sheng Lai,[†,‡,§] Maria Arielle Johnna Veronica Gaerlan Del Rosario,[†] Wei-Fu Chen,[†] Sheng-Che Yen,[†] Fei Pan,[∥,⊥] Qun Ren,[⊥] and Yen-Hsun Su*,[†]

[†]Department of Materials Science and Engineering, National Cheng Kung University, Tainan 70101, Taiwan

[‡]Institute of Physics, University of Münster, Wilhelm-Klemm-Strasse 10, Münster 48149, Germany

[§]CeNTech−Center for Nanotechnology, University of Münster, Heisenbergstrasse 11, Münster 48149, Germany

[∥]Physics Department, Technische Universität München, James-Franck-Straße 1, Garching 85748, Germany

[⊥]Laboratory for Biointerfaces, Swiss Federal Laboratories for Materials Science and Technology (EMPA), Lerchenfeldstrasse 5, St. Gallen 9014, Switzerland

ABSTRACT: In response to global energy shortage and global warming, liquid-type energy-yielding thermocells regulated by temperature differences are developed in this study, enabling generation of electric power from excess thermal energy or waste heat. The cells comprise nature pigments and wastewater. The cells are stable and functional within a narrow range of temperature difference, which can be as small as 40 °C. Under 40 °C temperature difference and with the solar cell size of 1 cm², daily energy generated by the designed solar cell can reach as high as 10022.4 KJ/m² in just 1 day, which is the highest energy-generation rate reported so far for the same type solar cells. The WS₂ nanosheet is utilized in liquid-type energy-yielding thermocells for assembly as water-splitting cells. When the pigments of Mona Lavender plectranthus are loaded into the electrolyte under a 40 °C temperature difference, the water-splitting cells demonstrated an energy conversion efficiency as high as 53.98% ± 4% for hydrogen evolution processing. Therefore, the dual fuction of the mini heat recycling system, e.g., power generation and hydrogen generation, has been achieved. Thus, the solar cells developed here have promising applications in recycling industrial waste heat and waste hot water.

KEYWORDS: liquid-type solar cells, AC impedance, halochromic pigments, thermal cell, water-splitting cell, recycling of waste heat, temperature difference
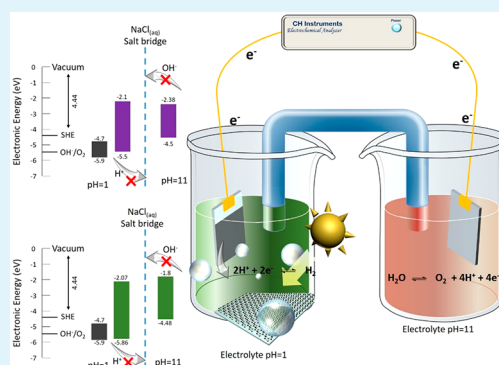
■ INTRODUCTION

With the increasing threat introduced by limited energy resources and global warming,[1] electrical power generation systems with environment friendly design and high efficiency are highly desired. Energy conversion and storage devices have thus attracted increasing attention.[2,3] Electrolytes are the most important and essential components in all types of batteries, including dyes-sensitive solar cells and water-splitting solar cells.[4,5] Among all gas molecules, hydrogen has the lightest molecular weight (2 g/mol) and highest energy density (enthalpy of −286 kJ/mol), which make it unreplaceable in green energy generation and conversion industry.[6,7] The most powerful device for hydrogen generation is hydrogen water-splitting cells.[3] Sandwich-structured water-splitting cells have been widely researched recently.[8−10] The anodes/cathodes are generally coated with semiconductor materials such as TiO₂, ZrO₂, ZnO, MoS₂, or WS₂ on indium tin oxide (ITO) glasses as the electron-collection layer and then further coated with photosensitizers as the light-absorption layer.[11−15] The conduction band and valence band energy levels of the sandwich-structured cells are expected to be higher than those of the standard hydrogen electrode (SHE) and lower than those of the hydroxyl oxidation.[11,16] Although the semiconductors with desired conduction band and valence band energy levels can be easily identified, the band gap of these semiconductor materials are still not satisfactory for water splitting. One of typical examples, ZrO₂, which is chemically highly stable, is able to absorb light with less than 213 nm wavelength excite electrons from valence band to conduction band, however, can only reach a band gap up to 5.8 eV.[17,18] Efforts have been made on searching for suitable photosensitizers as light-absorption anode by electron hopping.[19,20] Halochromic pigments are photosensitizers with various band gaps in the electrolytes having different pH values.[16] Organic halochromic pigments such as Methyl violet, methylene blue, methyl orange, and Congo red act as the photosensitizers in the ZrO₂-based water splitting solar cells.[16]

The highest hydrogen generation rate, however, only reached up to 1.8 mL/(h cm^2).[16] Most of the photosensitizers are designed with functional groups such as electron-donating groups and electron-accepting groups to be connected with normal semiconductor materials (metal-oxide) and to prevent the glut photosensitizers from dissolving into the electrolyte. Under most conditions, dissolution of photosensitizers into the electrolyte takes place.[16,21] Researchers have tried dissolving the photosensitizers into the electrolyte for creating power generating cells on purpose.

Two-dimensional (2D) materials have attracted much attention over the past ten years. molybdenum disulfide (MoS$_2$) and tungsten disulfide (WS$_2$) are intensively studied. In the literature,[22] the relationship between nanoscale hydrogen intercalation and the surface morphology and bandgap of two-dimensional (2D) α-MoO$_3$ nanosheets is demonstrated by local hydrogen ions intercalation behavior in α-MoO$_3$ nanoflakes. The local hydrogen ions are intercalated into MoO$_3$ and form H$_x$MoO$_3$ which reduce the band gap of MoO$_3$ and store the hydrogen ions. The authors Yichao Wang et al. demonstrated the excellent hydrogen generation efficiency in MoS$_2$ based photoinduced water-splitting cells.[23,24] These designs are reminiscent of the benefits and application of 2D semiconductor materials in electronic devices. When the Li$^+$ ions are introduced into the 2D MoS$_2$ host structure, the hydrogen evolution reaction is further enhanced by the Li$_x$MoS$_2$ compounds formation.[23] The results of EIS Nyquist plots of Li$_x$MoS$_2$ sample include, the reduction of charge-transfer resistance, enhancement of charge mobility, and the observance of high hydrogen generation efficiency. MoS$_2$ often suffers from rigorous conditions and tedious post-treatment whereas the latter usually produces quantum dots (QSs) with extremely low yield.[25,26] For utilizing our design in the quantum modulator cells in the near future, WS$_2$ would be our first candidate material for the water-splitting cells. Moreover, for fitting the energy levels of pigments under the electrolytes with various pH values, WS$_2$ demonstrated not only electrical, thermal, and chemical stability but also the fitted conduction band energy level (-4.7 eV) and valence band energy level (-5.9 eV) with reference to the vacuum energy level.[13−15]

The waste heat is also the big environmental pollution. Recently, thermocells prepared by electrodes coated with ferricyanide derivatives (K$_3$Fe(CN)$_6$)/ (NH$_4$)$_4$Fe(CN)$_6$) and Pt were used to recycle the wasted heat that is generated from industry, solar, or air conditioners. The maximum cell power (P_{max} of 30960 KJ/m^2 for 1 day)[27,28] were reported under electrolytes within a 150 °C temperature difference. The ferricyanide derivatives of the thermocell are not only utilized to create the unbalancing chemical potential in the separated electrolytes but also act as the photosensitizers in the dye-sensitized solar cell.[29] However, for the thermocells, the photoinduced electron excitation needs to be taken into consideration.

Basically, the dissolution of the pigments (photosensitizers) into the electrolytes on a sandwich-structured water-splitting cell cannot be prevented, leading to failure in sustaining the high efficiency of the cells.[11,16] The reported efficiencies of thermocells that contain pigments dissolved in electrolytes are not the effective efficiencies because the effect of the photoinduced excited electrons is not taken into consideration. Furthermore, the dual system for hydrogen generation and power generation simultaneously has rarely been reported. Much effort has been dedicated to developing high-performance water-splitting cells or solar cells.
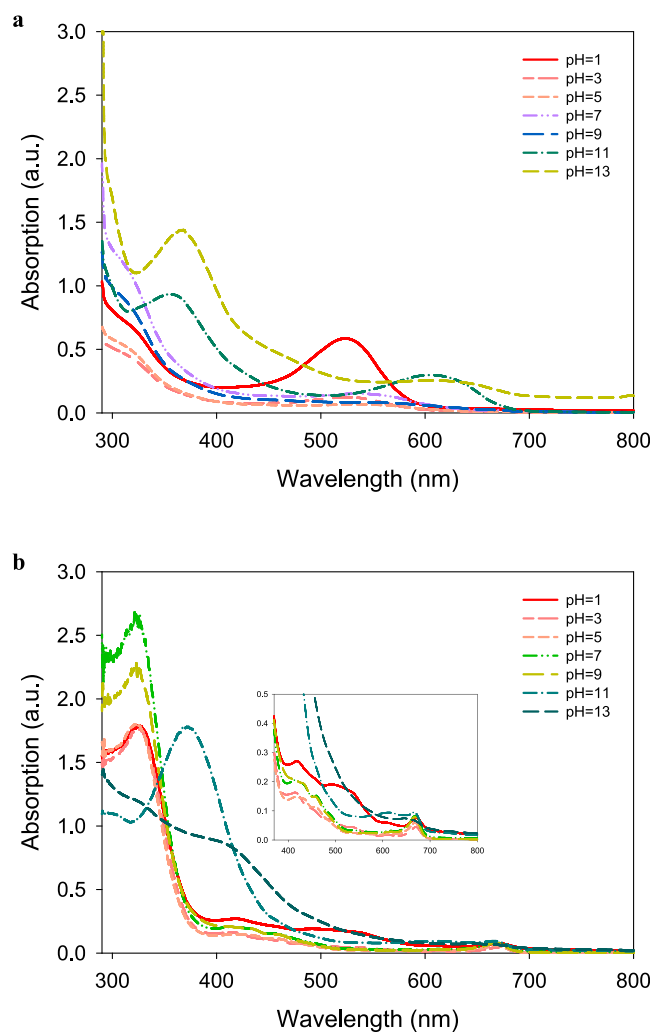

Figure 1. Absorption spectrum of (a) G-anthocyanin and (b) Mona Lavender plectranthus in the solution with different pH values.
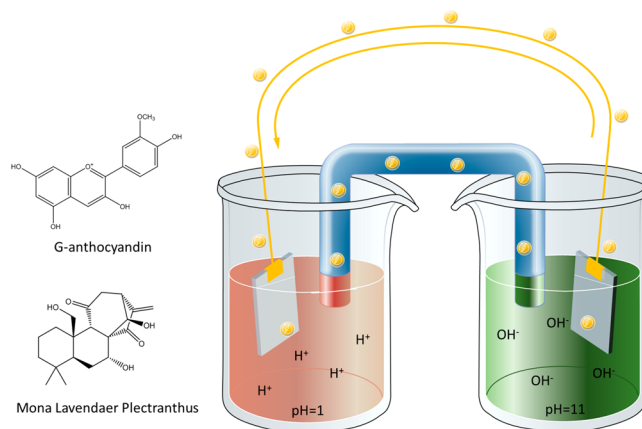

Figure 2. Molecular structure of G-anthocyandin and Mona Lavendaer plectranthus and the structure of liquid-type energy-yielding thermocell.

Thus, in this work, natural halochromic pigments are formatted into electrolytes at various pH in the system of liquid-type energy yielding thermocells to create unbalanced chemical potential and to modulate the energy level of electrolytes by the photoinduced electron excitation. The same system is further transferred into the water splitting and hydrogen
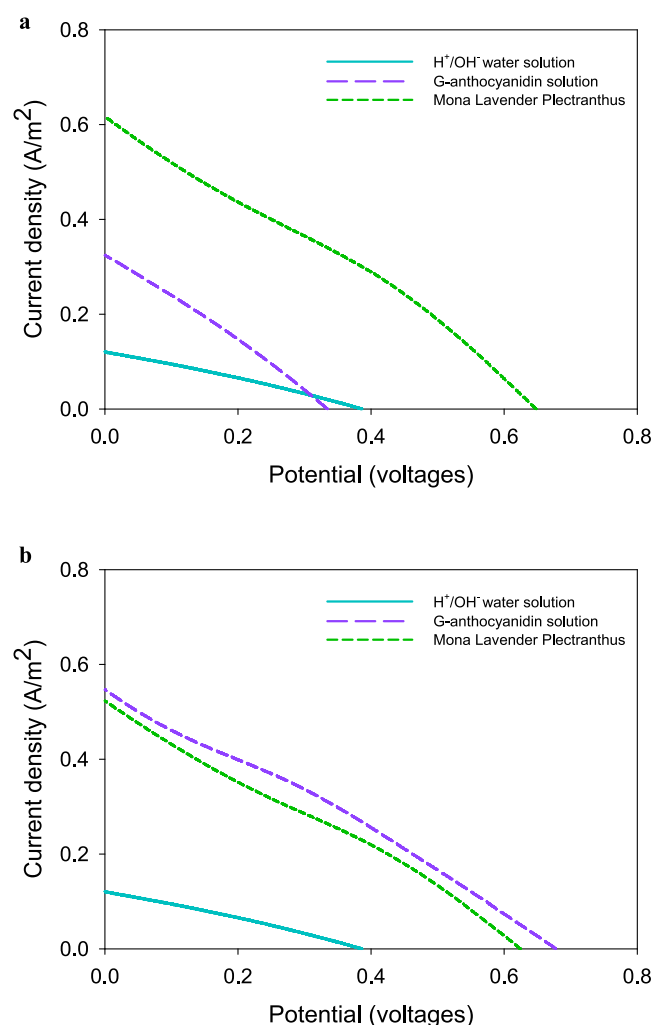
Figure 3. $J-V$ curve of liquid-type energy-yielding thermocells at room temperature in (a) dark field and (b) bright field with G-anthocyanin and Mona Lavender plectranthus loading.

Figure 4. $J-V$ curve of liquid-type energy-yielding thermocells maintained at 40 °C temperature different in (a) dark field and (b) bright field with G-anthocyanin and Mona Lavender plectranthus loading.

evolution cells when the semiconductor material with suitable energy level is coated on the anode electrode. The properties of photoinduced electron excitation are also studied, when the photosensitizer dissolves into the electrolyte under suitable light irradiation. The electron hopping step, with ground state between standard hydrogen electrode (SHE) and hydroxyl oxidation energy level, is generated when the excited energy level is much higher than SHE. Thus, the liquid-type energy-yielding thermocell systems based on hydrogen-evolution water-splitting cells were introduced by suitable preparation of semiconductor anodes and natural halochromic pigments loaded electrolyte under solar light irradiation. As a result, the
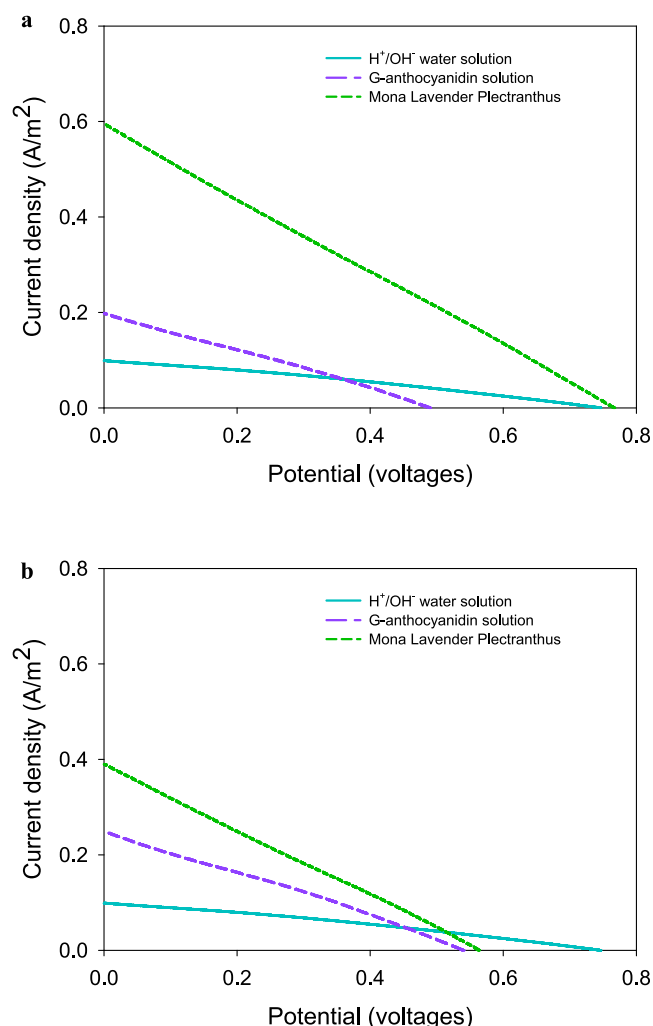
energy-yielding thermocells with a water-splitting dual system is designed and assembled by the natural halochromic photosensitizers within various pH electrolytes and narrow temperature difference under solar light irradiation. The green energy conversion and generation design is able to reuse mini heat from the environment to decompose the wastewater into hydrogen gases for environmental protection.

■ EXPERIMENTAL SECTION

Electrolytes. The electrolytes with different pH values were prepared by hydrochloric acid (HCl, 38%, Sigma-Aldrich) and sodium hydroxide

Table 1. Properties of Liquid-Type Energy-Yielding Thermocell at Room Temperature in Dark Field (D) and Bright Field (L)[a]

	J_{sc} (A/m²)	V_{oc} (V)	J_{op} (A/m²)	V_{op} (V)	power max (W/m²)	ff
H⁺/OH⁻ water solution electrolytes	0.12 ± 0.031	0.39 ± 0.052	0.067 ± 0.082	0.20 ± 0.072	0.013 ± 0.005	0.278 ± 0.023
D: G-anthocyandin	0.32 ± 0.082	0.34 ± 0.108	0.17 ± 0.112	0.18 ± 0.091	0.031 ± 0.008	0.278 ± 0.019
D: Mona Lavender plectranthus	0.62 ± 0.121	0.65 ± 0.171	0.30 ± 0.137	0.39 ± 0.142	0.117 ± 0.081	0.275 ± 0.027
L: G-anthocyandin	0.55 ± 0.158	0.68 ± 0.143	0.29 ± 0.091	0.36 ± 0.110	0.104 ± 0.052	0.285 ± 0.035
L: Mona Lavender plectranthus	0.52 ± 0.112	0.63 ± 0.152	0.36 ± 0.088	0.25 ± 0.177	0.090 ± 0.0023	0.298 ± 0.021

[a]H⁺/OH⁻ water solution electrolytes: the electrolyte of liquid-type energy-yielding thermocell cells use only H⁺/OH⁻ water solution; G-anthocyandin: the electrolytes of liquid-type energy-yielding thermocells are loaded with G-anthocyandin; Mona Lavender plectranthus: the electrolytes of liquid-type energy-yielding thermocells are loaded with Mona Lavender Plectranthus. (Every result is tested under at least 10 samples).

Table 2. Properties of Liquid-Type Energy-Yielding Thermocell with 40 °C Temperature Difference in Dark Field (D) and Bright Field (L)[a]

	J_{sc} (A/m^2)	V_{oc} (V)	J_{op} (A/m^2)	V_{op} (V)	power max (W/m^2)	ff
H$^+$/OH$^-$ water solution electrolytes	0.10 ± 0.005	0.75 ± 0.023	0.06 ± 0.018	0.4 ± 0.029	0.024 ± 0.011	0.320 ± 0.047
D: G-anthocyandin	0.25 ± 0.031	0.49 ± 0.068	0.1 ± 0.020	0.27 ± 0.041	0.027 ± 0.032	0.220 ± 0.027
D: Mona Lavender Plectranthus	0.60 ± 0.058	0.77 ± 0.028	0.29 ± 0.013	0.4 ± 0.025	0.116 ± 0.081	0.251 ± 0.056
L: G-anthocyandin	0.20 ± 0.017	0.54 ± 0.052	0.13 ± 0.030	0.29 ± 0.011	0.038 ± 0.013	0.352 ± 0.083
L: Mona Lavender Plectranthus	0.39 ± 0.023	0.56 ± 0.037	0.19 ± 0.021	0.29 ± 0.019	0.055 ± 0.020	0.252 ± 0.097

[a]H$^+$/OH$^-$ water solution electrolytes: the electrolyted of liquid-type energy-yielding thermocells use only H$^+$/OH$^-$ water solution; G-anthocyandin: the electrolytes of liquid-type energy-yielding thermocell are loaded with G-anthocyandin; Mona Lavender plectranthus: the electrolytes of liquid-type energy-yielding thermocells are loaded with Mona Lavender pPlectranthus. Every result was tested with at least 10 samples.
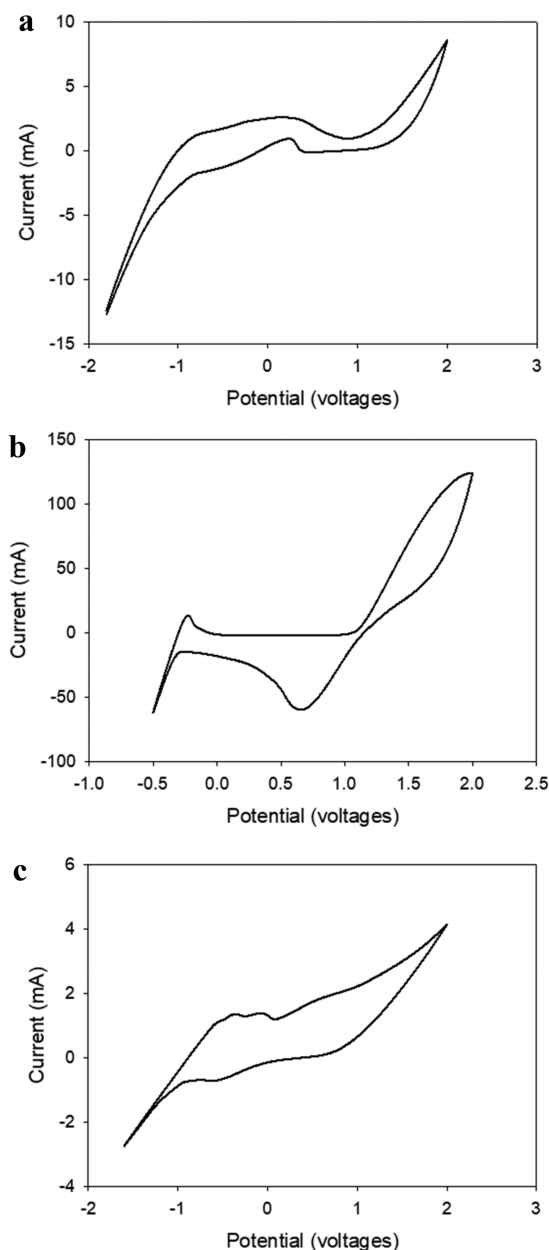

Figure 5. Cyclic voltammograms of G-anthocyanin in (a) 0.1 M LiClO$_4$ acetonitrile solution, (b) HCl water solution with pH of 1, and (c) NaOH water solution with pH of 11. The CV rate was 50 mV/s (vs Ag/Ag$^+$).

Figure 6. Cyclic voltammograms of Mona Lavender Plectranthus in (a) 0.1 M LiClO$_4$ acetonitrile solution, (b) HCl water solution with pH of 1, and (c) NaOH water solution with pH of 11. The CV rate was 50 mV/s (vs Ag/Ag$^+$).

(NaOH, purity ≥97%, Sigma-Aldrich) water solution. The salt bridge was prepared by 1 M sodium chloride (NaCl, Sigma-Aldrich) solution.
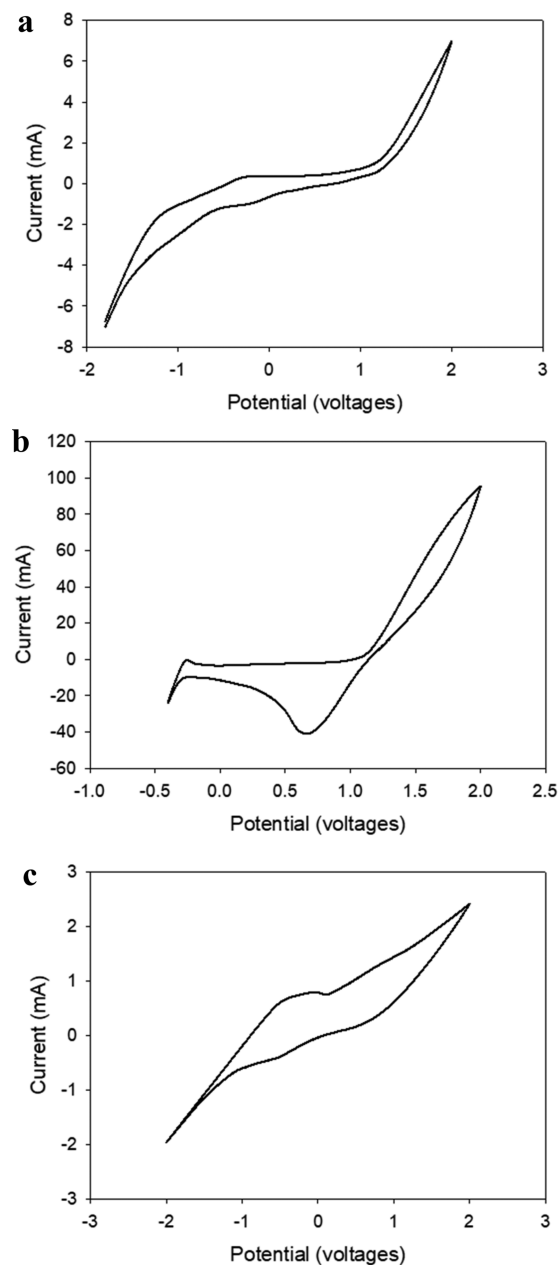
Electrodes for Thermocells. The Pt foils (1 cm^2 with 1 mm thick, AF Chemicals) were used to serve as the anode and cathode electrode.

Electrodes for Water Splitting Cells. The Pt foils (1 cm² with 1 mm thick, AF Chemicals) were used to serve as the cathode electrode. Tungsten(IV) sulfide (WS₂, powder, 2 μm, 99%, Sigma-Aldrich) was used as semiconductor material in the water-splitting cells system. The powder WS₂ (0.5 g) were prepared as suspension solution within ethanol solvent (20 mL) (99.5%, spectrum grade, Fisher Scientific). Precleaned Indium Tin Oxide (ITO, surface resistivity 8–12 Ω/sq, Sigma-Aldrich) was dipped in the WS₂ suspension solution (1 mL/cm²). These coated glasses were then used as anode electrodes in the water-splitting cell system.

Photosensitizers. Natural anthocyanidin (G-anthocyanidin) and pigment of Mona Lavender plectranthus (MLP), used as photosensitizers in this work, were extracted from grapes and Mona Lavender plectranthus. In more detail, 50 g of dried grape peers and dried Mona Lavender plectranthus leaf were soaked in 1000 mL of 100% ethanol to extract G-anthocyanidin and MLP by rotary evaporators under 70 °C for 1 h, respectively. Both G-anthocyanidin and MLP solutions were concentrated in 800 mL of ethanol solution after the evaporation of ethanol.

Cell Structure. In this work, the cells were constructed as follows: two individual electrolytes were connected through NaCl$_{(aq)}$ salt bridge. One Pt foil was settled into the acid electrolyte and acted as the anode electrode, and another one into the base electrolyte and as the cathode electrode.

Characterization. UV–vis absorption spectrum was measured by the spectrophotometer (CT-2200, ChromTech), and a quartz container with light path of 1 cm was used to analyze absorption spectrum.

Electrochemical analysis including current–voltage characterization (*J–V* curves) and the electrochemical impedance spectroscopy (EIS) were performed by using CH Instruments (6273E, CH Instruments, Inc.).

The bright and dark fields used for analyzing the photoinduced performance of the liquid-type energy-yielding thermocells and water-splitting cells were modulated in a dark room with or without the AM 1.5G irradiation, respectively.

A D8 Discover with a general area diffraction detection system (Bruker AXS Gmbh, Karlsruhe, Germany) was utilized to obtain X-ray diffraction patterns to analyze the crystallinity of WS₂.

Optical microscope (OM) image analyzation was completed using Olympus BX51M.

The Raman spectrum was measured by the Horiba Jobin Yvon Raman microscope.

The X-ray photoelectron spectroscopy (XPS) spectrum of WS₂ was measured by an X-ray photoelectron spectrometer (Thermo Scientific, Theta Probe).

■ RESULTS AND DISCUSSION

Optical Properties of G-Anthocyanin and Mona Lavender Plectranthus (MLP) as Photosensitizers. G-anthocyanin and MLP were first investigated for their absorption spectrum in a range of ultraviolet to visible light (Figure 1). Halochromic pigments, G-anthocyanin and MLP were color-variable in solutions with different pH. G-anthocyanin displayed red color in solution of low pH, as indicated in Figure 1. A sharp peak was observed at 530 nm in HCl water solution having pH 1 (Figure 1a). In solutions with high pH, G-anthocyanin displayed colors of green and blue. An obvious peak was found at 613 nm in NaOH water solution having pH 11 (Figure 1a). MLP exhibited a similar trend to G-anthocyanin. The acidic water solution turned the MLP solution into red and the alkaline water solution turned the MLP into green and blue (Figure 1b). When MLP dissolved into the HCl water solution at pH 1, many peaks were observed in the UV–vis regime, which were generated by exciting the electrons from ground state to excited state. The most obviously one is shown at 540 nm. A sharp peak at 377 nm appeared when MLP dissolved in the NaOH solution at pH 11. Thus, both G-anthocyanin and MLP showed clear absorption in the UV–vis region, demonstrating both can be good candidates as photosensitizers in electrolytes
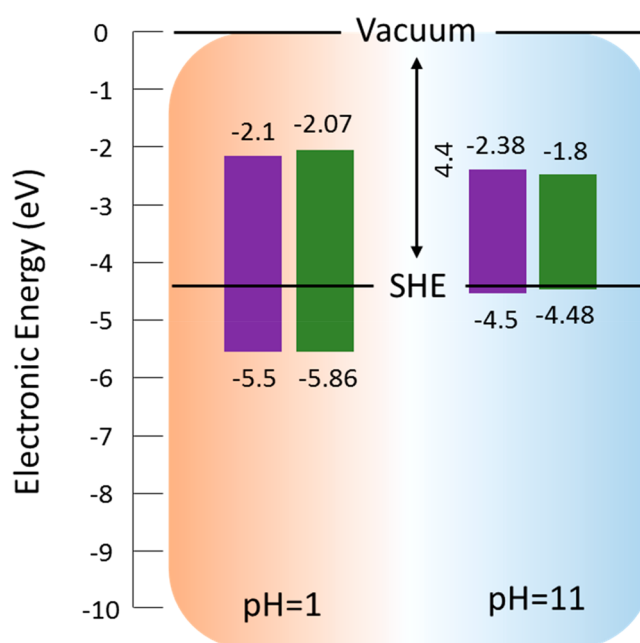

Figure 7. Vacuum energy level of the natural halochromic pigments in the electrolytes with different pH. SHE: −4.44 eV vs vacuum.
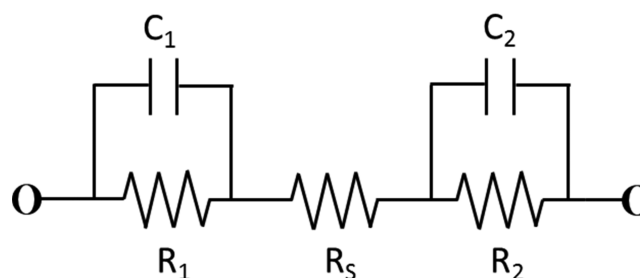

Figure 8. Equivalent electrical analogs. R_S is the total resistance of the interface between Pt films and the electrolytes. C_1 and R_1 are the capacity and the resistance of the HCl water solution, C_2 and R_2 are the capacity and the resistance of the NaOH water solution.

with various pH values for efficiency enhanced liquid-type energy-yielding thermocells and water-splitting cells by photoelectrochemical conversion.

Liquid-Type Energy-Yielding Thermocells. To further explore G-anthocyanin and MLP as photosensitizers, we assembled liquid-type energy-yielding thermocells, as illustrated in Figure 2. The electrons were generated from the concentration difference of H⁺/OH⁻ in water solutions and natural halochromic pigment-absorbed light. Combining the electromotive force (EMF) equation with the simplest acid–base concentration-difference (H⁺/OH⁻) cell, eq 1 is derived, where concentration is the bottleneck to increasing power efficiency and the temperature is a critical factor affecting the electrical potential of the cell.

$$\varepsilon = \varepsilon^{\circ} - \frac{RT}{zf}\ln \frac{c_{H_2O}}{c_{H^+}c_{OH^-}} \qquad (1)$$

where ε is the potential of the cell, ε° is the chemical potential of water formation, R is the gas constant, T is temperature in Kelvin (K), z is the electrons in the reaction, f is the Faraday's constant, c_{H_2O} is the concentration of water, c_{H^+} is the concentration of H⁺, and c_{OH^-} is the concentration of OH⁻.
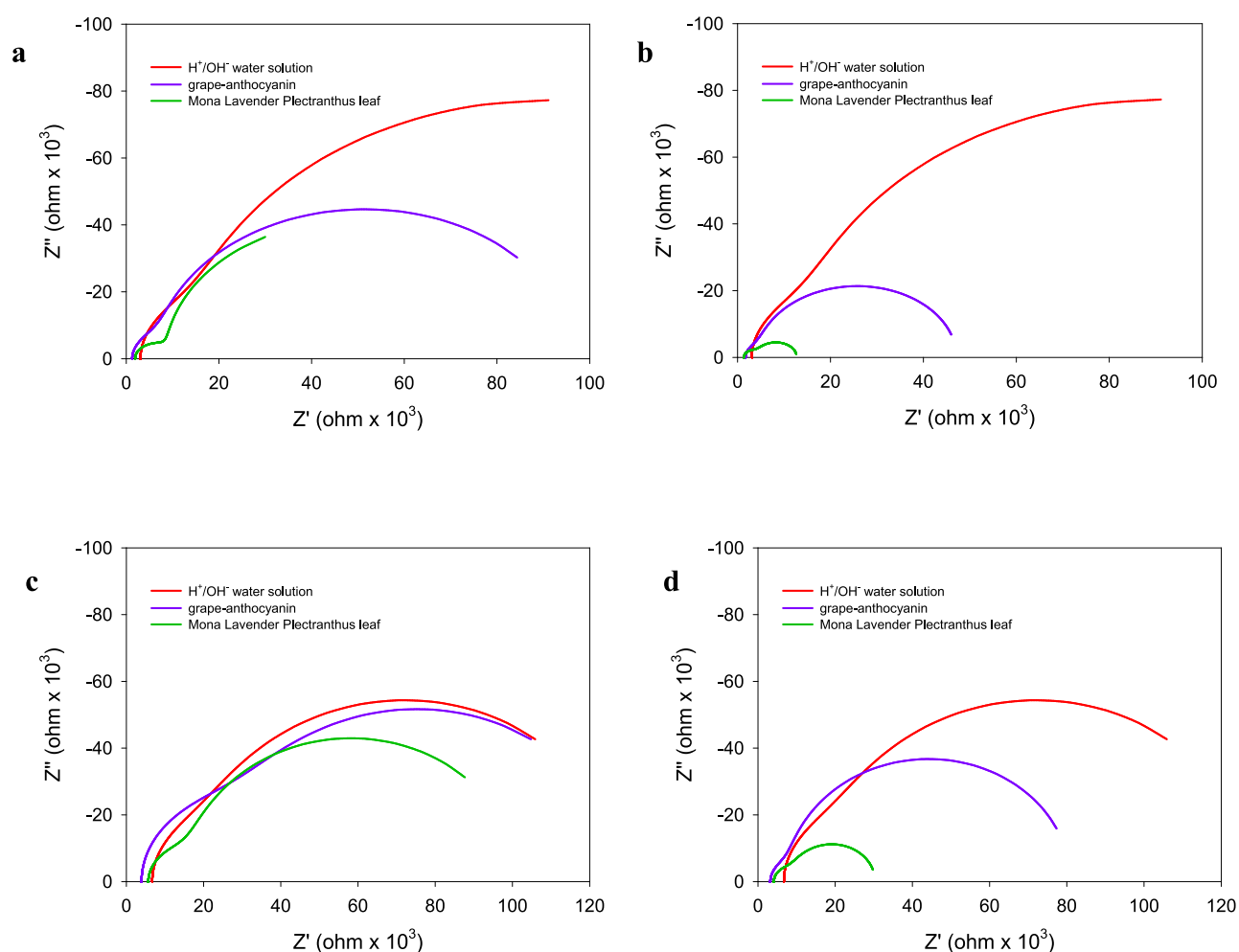
Figure 9. Nyquist diagram of the liquid-type energy-yielding thermocells under different conditions: (a) dark field and room temperature, (b) bright field and room temperature, (c) dark field and temperature difference of 40 °C, and (d) bright field and temperature difference of 40 °C.

Table 3. Electron Diffusion Phenomenon of the Liquid-Type Energy-Yielding Thermocells at Temperature Difference (dT) of 0 °C, Temperature Difference (dT) of 40 °C, Dark Field (D) and Bright Field (L)[a]

	R_S (Ω m)	σ (S/m)	D (m²/s)	R_1(Ω m)	C_1 (F)	R_2(Ω m)	C_2 (F)
RT: H⁺/OH⁻ water solution electrolytes	6707 ± 335	0.15 ± 0.03	0.01 ± 0.002	14330 ± 597	3.48 ± 0.57 × 10⁻⁵	105600 ± 1872	3.76 ± 0.83 × 10⁻⁵
RTD: G-anthocyandin	4128 ± 217	0.24 ± 0.05	0.02 ± 0.005	88720 ± 932	5.08 ± 0.43 × 10⁻⁵	6158 ± 324	5.20 ± 0.57 × 10⁻⁵
RTD: Mona Lavender plectranthus	3213 ± 163	0.31 ± 0.08	0.02 ± 0.004	6475 ± 319	8.96 ± 0.92 × 10⁻⁵	102600 ± 1367	1.24 ± 0.22 × 10⁻⁴
RTL: G-anthocyandin	1727 ± 153	0.58 ± 0.19	0.04 ± 0.002	42360 ± 405	7.02 ± 0.83 × 10⁻⁵	3027 ± 157	1.06 ± 0.19 × 10⁻⁴
RTL: Mona Lavender plectranthus	1370 ± 107	0.73 ± 0.25	0.05 ± 0.004	2910 ± 115	6.20 ± 0.32 × 10⁻⁵	8502 ± 412	1.00 ± 0.21 × 10⁻⁴
dT: H⁺/OH⁻ water solution electrolytes	5705 ± 233	0.18 ± 0.04	0.01 ± 0.002	12980 ± 432	4.98 ± 0.33 × 10⁻⁵	15270 ± 113	3.82 ± 0.43 × 10⁻⁵
dTD: G-anthocyandin	3944 ± 198	0.25 ± 0.07	0.02 ± 0.003	10650 ± 323	5.00 ± 0.36 × 10⁻⁵	84820 ± 817	5.16 ± 0.61 × 10⁻⁵
dTD: Mona Lavender plectranthus	3071 ± 127	0.33 ± 0.11	0.02 ± 0.005	97350 ± 871	8.73 ± 0.87 × 10⁻⁵	26060 ± 273	2.31 ± 0.29 × 10⁻⁴
dTL: G-anthocyandin	1287 ± 112	0.78 ± 0.23	0.05 ± 0.007	4665 ± 462	5.52 ± 0.61 × 10⁻⁵	21580 ± 281	7.43 ± 0.81 × 10⁻⁵
dTL: Mona Lavender plectranthus	1143 ± 131	0.87 ± 0.19	0.06 ± 0.004	73030 ± 517	5.95 ± 0.73 × 10⁻⁵	4715 ± 214	8.16 ± 0.93 × 10⁻⁵

[a]H⁺/OH⁻ water solution electrolytes: only H⁺/OH⁻ water solution applied in the electrolytes of liquid-type energy-yielding thermocells; G-anthocyandin: the electrolytes of liquid-type energy-yielding thermocells were loaded with G-anthocyandin; Mona Lavender plectranthus: the electrolytes of liquid-type energy-yielding thermocells were loaded with Mona Lavender plectranthus. Every result was tested with at least 10 samples).

The current density of the liquid-type energy-yielding thermocells in G-anthocyanin or MLP loaded H⁺/OH⁻ water solutions were investigated for the current density–voltages spectrum ($J–V$ curve) (Figure 3 and Table 1). The short circuit current density (J_{sc}) of the H⁺/OH⁻ solution in the thermocell was measured to be 0.12 A/m², and the open circuit voltage (V_{oc}) was 0.39 V (Table 1). The maximum power of H⁺/OH⁻ solutions was 0.013 W/m², where voltage (V_{op}) and current
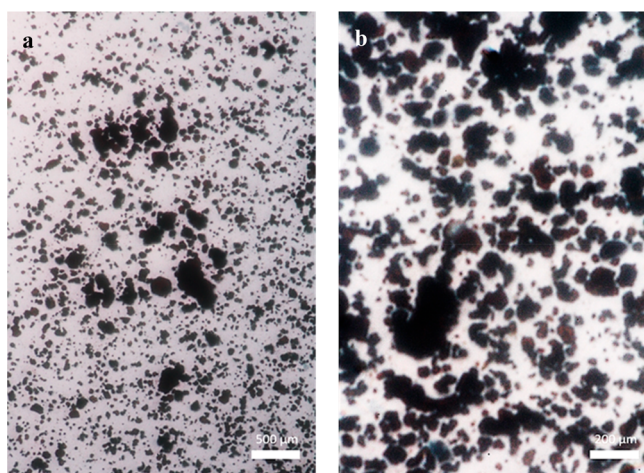
Figure 10. Optical microscope images of WS$_2$. (a) 40× and (b) 100×.

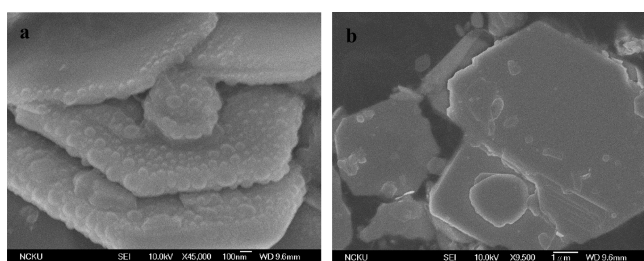**Figure 11.** SEM images of the WS$_2$-coated ITO substrates. (a) Tilt 45° and (b) top view.

density (J_{op}) were found to be 0.20 V and 0.066 A/m^2, respectively (Table 1). Both G-anthocyanin and MLP-loaded H$^+$/OH$^-$ solutions were able to increase the power of the thermocell dramatically (Figure 3). In the dark field, the maximum power of the G-anthocyanin loaded thermocell was measured to be 0.031 W/m^2 (V_{op} of 0.18 V and J_{op} of 0.17 A/m^2), whereas the J_{sc} and V_{oc} were 0.32 A/m^2 and 0.34 V, respectively. Interestingly, the MLP-loaded thermocell demonstrated even higher power generation than the G-anthocyanin-loaded one. The maximum power was found to be 0.117 W/m^2 (J_{sc} of 0.62 A/m^2 and V_{oc} of 0.65 V) when V_{op} reached 0.39 V and J_{op} reached 0.30 A/m^2.

In the bright field, where the thermocell was illuminated with AM 1.5G irradiation, the current density of the short circuit and the open circuit voltage of G-anthocyanin loaded thermocell rose dramatically (Figure 3b, Table 1). The J_{sc}, V_{oc}, and maximum power were as high as 0.55 A/m^2, 0.68 V, and 0.104 W/m^2, respectively. In contrast, the maximum power, J_{sc} and V_{oc} of MLP loaded thermocell did not differ much from those measured in the dark field, and were found to be 0.09 W/m^2 (voltage of 0.36 V and current density of 0.25 A/m^2), 0.52 A/m^2, and 0.63 V, respectively.

The photo excited electrons from both G-anthocyanin and MLP provided thermocells with obviously enhanced power. Thus, both G-anthocyanin and MLP are demonstrated to be suitable photosensitizers for usage in thermocells.

Temperature-Difference-Induced Electromotive Force (EMF) of the Liquid-Type Energy-Yielding Thermocells. The large temperature difference induces higher generated power than the small temperature difference.[27] The maximum temperature for creating the widely temperature is as high as 150 °C, which is over the normal civic environment with. The liquid-type energy-yielding thermocells with temperature factor
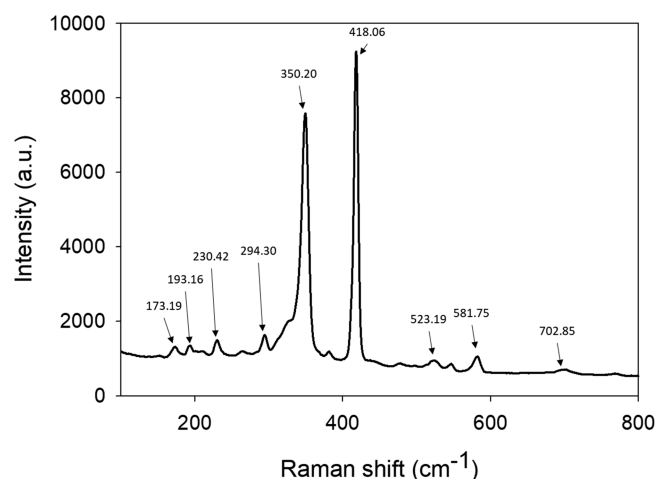

Figure 12. Raman spectra from a WS$_2$ region at room temperature (514.5 nm laser excitation).
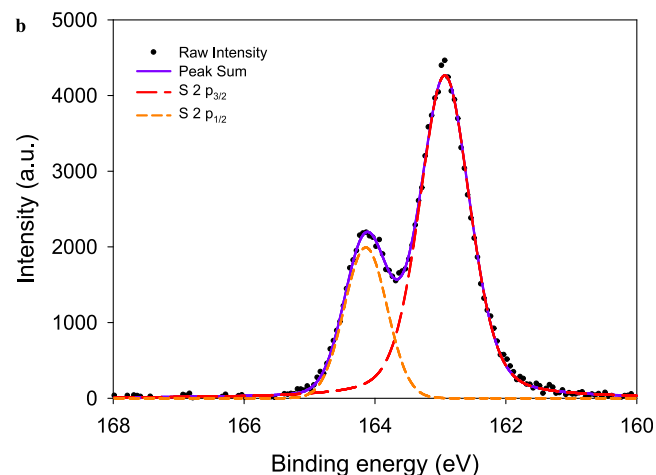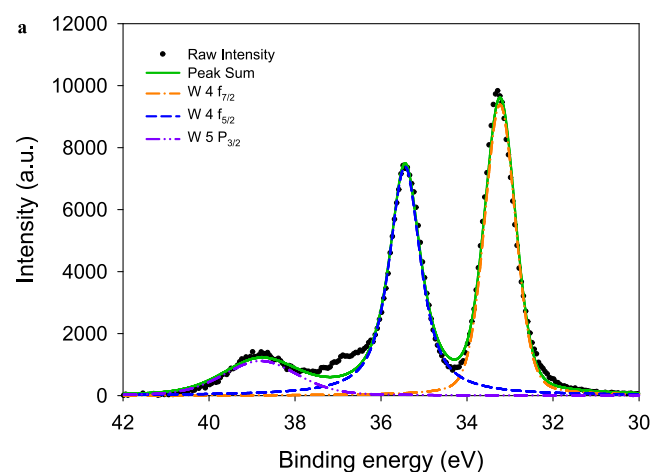

Figure 13. XPS scan of (a) W 5p and W 4f and (b) S 2p for WS$_2$.

were designed (Figure 4). For operating the liquid-type energy-yielding thermocells within narrow temperature difference, the H$^+$ and OH$^-$ solutions were sustained at 50 and 10 °C, respectively. This temperature-difference induced a higher power in the H$^+$/OH$^-$ solutions compared with the thermcell kept at the same room temperature. The maximum power was 0.024 W/m^2 (voltage of 0.40 V and the current density of 0.06 A/m^2) and the
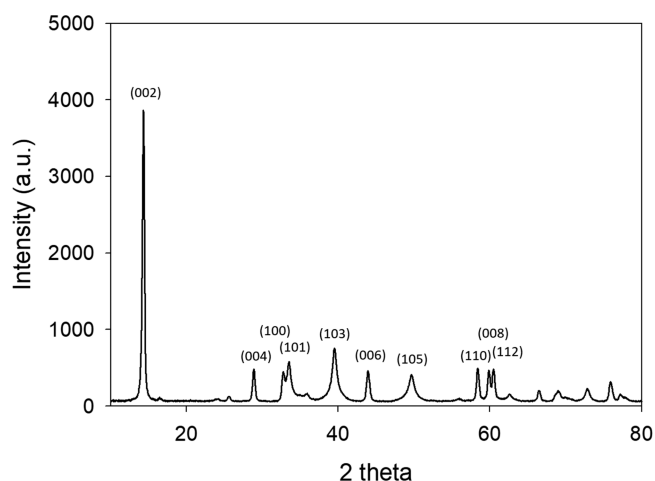
Figure 14. XRD patterns of WS_2 (JCPDS card no. 85−1068).

J_{sc} and the V_{oc} were 0.10 A/m^2 and 0.75 V, respectively. Both max power and V_{oc} reached the values almost doubled those obtained at room temperature.

The G-anthocyanidin or MLP-loaded thermocells also showed higher power than those obtained at the room temperature. In the dark field, the power of the G-anthocyanidin- and MLP-loaded thermocells were 0.026 W/m^2 (voltage of 0.27 V and the current density of 0.097 A/m^2) and 0.116 W/m^2 (voltage of 0.4 V and current density of 0.29 A/m^2), respectively (Figure 4a, Table 2), similar to those measured in dark at room temperature. In the bright field, G-anthocyanidin loaded thermocell showed higher power (Power$_{max}$ of 0.038 W/m^2, voltage of 0.29 V, and current density of 0.13 A/m^2) than in the dark field (Figure 4b, Table 2).

Figure 3 demonstrates the results of electrolytes without temperature difference under bright and dark field. These $J−V$ curves demonstrate that current density and power efficiency are enhanced by light irradiation. Figure 4 demonstrates the results of electrolytes with temperature difference. From the J-V curves, the temperature difference induced sample demonstrated higher current density compared to the cells in the conditions without temperature difference. These phenomena become more prominent in the case of H+/OH− water solution electrolytes and G-anthocyandin. Thus, the temperature effect is proved to have a positive contribution to the mini heat recycling thermocells.

Estimated Energy Level and Band-Gap Determination. According to the above result, the band gaps of these natural halochromic pigments can be controlled by solutions having different pH. The cyclic voltammetry (CV) curves of these natural halochromic pigments in 0.1 M LiClO$_4$ ACN solution, HCl water solution with pH of 1 and NaOH water solution with pH of 11 are shown in Figures 5 and 6. Corresponding with the UV−vis spectrum, excited state and ground state energy levels were determined and are shown in Figure 7.

The band gap of G-anthocyanidin HCl water solution at pH 1 was 3.4 eV and NaOH water solution at pH 11 was 2.12 eV. According to that, the excited photoelectrons were easily generated by light irradiation. As the working electrode was settled in the G-anthocyanidin-loaded NaOH water solution (pH 11) which contained high concentration OH$^-$ groups, the electrons migrate from NaOH solution to HCl solution rather than the inverse migrated direction. The MLP loaded thermocells demonstrated the higher power in the dark field than that in the bright field. The band gap of PLP pigments in HCl water solution (pH of 1) was 3.79 eV and in NaOH water solution (pH of 11) was 2.68 eV. Since MLP generated photoelectrons by absorbing the light irradiation, the photoelectrons in the NaOH water solution (pH of 11) oxidized OH$^-$
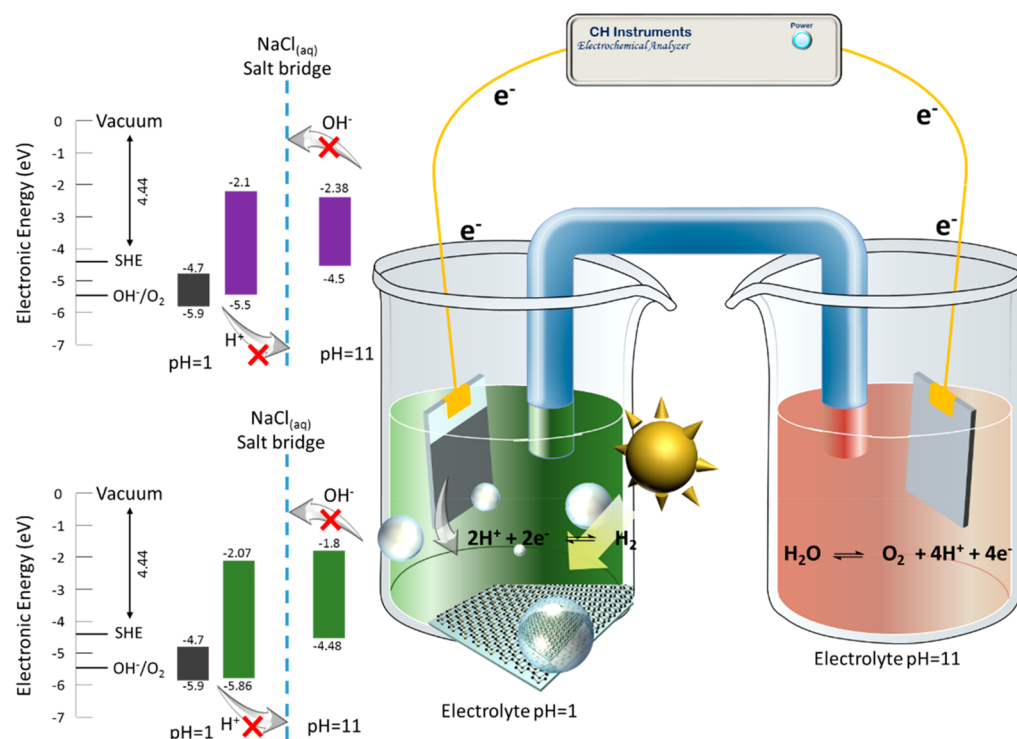

Figure 15. Water-splitting system of halochromic pigment-loaded electrolytes. Cathode, Pt foil (1 cm^2 with 1 mm thick); anode, WS_2-coated ITO substrates; and NaCl(aq) salt bridge.

ions into oxygen and the photoelectron in HCl water solution (pH of 1) reduced H^+ ions into hydrogen. With increasing time of the light irradiation on the MLP pigment-loaded thermocell, the power and the current density of the system decreased drastically and there were bubbles generated from NaOH water solution and HCl water solution. Furthermore, the pH value of the MLP loaded water solution changed rapidly, with the pH of the NaOH water solution and the HCl water solution switching from 11 to 7.4 and from 1 to 5 in 30 s, respectively.

Electron Diffusion Analysis of the Established Thermocells. To determine the electron diffusion phenomena and diffusion coefficient calculation, we utilized the spectrum analysis of electrochemical impedance by the equivalent electrical analogs to determine the electron diffusion phenomena in Figure 8. R_S is the total resistance of the interface between Pt films and the electrolytes. C_1 and R_1 are the capacity and the resistance of the HCl water solution with pH of 1, respectively. C_2 and R_2 are the capacity and the resistance of the NaOH water solution with pH of 11, respectively. The migration path was determined from the R_S and the following equation.

The electron mobility (μ) was determined by eq 2

$$\sigma = \mu n q \qquad (2)$$

where σ is the electric conductivity (S/m), n is the ion concentration, q is the electricity (1.6×10^{-19} C). The diffusion coefficient of the electrons in the liquid-type energy-yielding thermocell was determined by eq 3

$$D = \mu k_B T / e \qquad (3)$$

where k_B is the Boltzmann constant (1.38×10^{-23} J/K) and T is the Kelvin temperature.

Figure 9 shows the Nyquist diagram of the G-anthocyanidin and MLP loaded thermocells in dark and bright field at room temperature. The resistance of the thermocell was reduced with G-anthocyanidin and MLP loaded the electrolyte when the system is in bright field compared to that in the dark field. As the G-anthocyanidin- and MLP-loaded thermocells absorbed light, the resistance in light was lower than that in the dark field. The photoinduced thermocells effectively increased the power of photoelectron generation by natural halochromic pigments. On the basis of the detailed calculation of electron diffusion in the thermocells presented in Table 3, the ideal parameters of the thermocell setting were listed. The temperature difference induced a lower interface resistance between Pt films and the electrolytes than the electrolytes of thermocell at the room temperature. In general, the natural pigments loaded thermocell has higher electron mobility and electron diffusion coefficient than the nonloaded electrolytes. The electron diffusion coefficient at the interface between Pt films and the electrolytes of MLP loaded thermocell was six times higher than that of H^+/OH^- water solution, which induced higher power of this system than the so-far reported Liquid-type energy-yielding thermocells. The natural halochromic pigments generated photoelectrons by absorbing irradiation from AM 1.5 G. Thus, bright fields allow higher pigments load than the dark fields. MLP-loaded thermocell demonstrated the opposite state because the photoelectrons from MLP oxidized OH^- ions into oxygen and reduced H^+ ions into hydrogen in the basic and acidic water solution electrolytes, respectively.

Water-Splitting Cell System. Two-dimension semiconductor materials such as graphene, MoS_2 and WS_2 are promising and popular semiconductors in hydrogen generation industry.[13,15] The sheet-likelihood structure with thickness of several
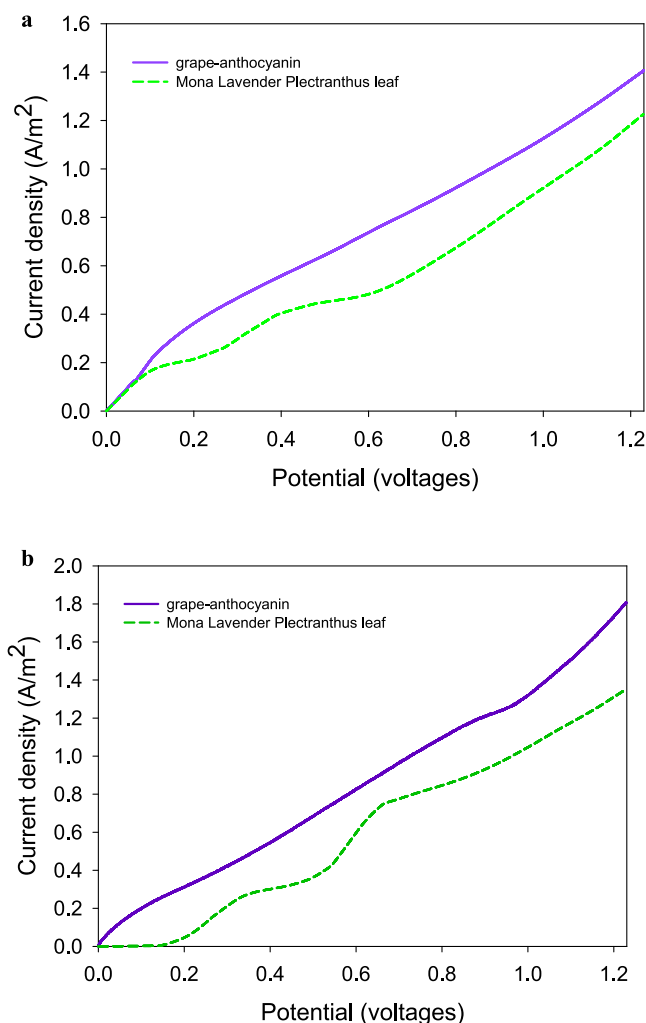
Figure 16. Current density of WS_2-based water splitting within halochromic pigment-loaded electrolytes under AM 1.5G irradiation. (a) Electrolytes with temperature difference of 0 °C and (b) electrolytes with temperature difference of 40 °C.

Å provided the material with excellent electrical and thermal stability.[30] The WS_2 nanosheets were stable at the high working temperature (over 1000 °C).[31]

From the optical microscope images of WS_2 in Figure 10, the dispersion WS_2 on the ITO substrates is around 2−3 μm. The SEM images of exfoliated flakes WS_2 are demonstrated in Figure 11, in which the thickness of a WS_2 nanosheet is 100 ± 10 nm and the lateral dimension is 1.5 ± 0.3 μm. The Raman spectrum of WS_2 is plotted in Figure 12. Under the 514.5 nm laser excitation, the characteristic peaks at 348.9 and 418.1 cm^{-1} are obviously demonstrated, which agrees with results from the literature.[32,33] The X-ray photoelectron spectroscopy (XPS) of WS_2 that is utilized in this manuscript has been plotted in the Figure 13. The binding energy and the relatively intensity indicate that there are pure WS_2 detected in XPS spectrum. From Figure 13a, the peaks of W $4f_{7/2}$, W $4f_{5/2}$, and W $5p_{3/2}$ are located at binding energy 33.28, 35.48, and 38.78 eV, respectively. From Figure 13b, the peaks of S $2p_{1/2}$ and S $2p_{3/2}$ are located at binding energy 164.18 and 162.98 eV, respectively. These XPS results agree with those in the literature.[34] The pure orthorhombic X-ray diffraction pattern of WS_2 is demonstrated in Figure 14. The phase of WS_2 is fitted with JCPDS card no. 85−1068 and the crystallinity of WS2 is as high as 97.6%.[33]
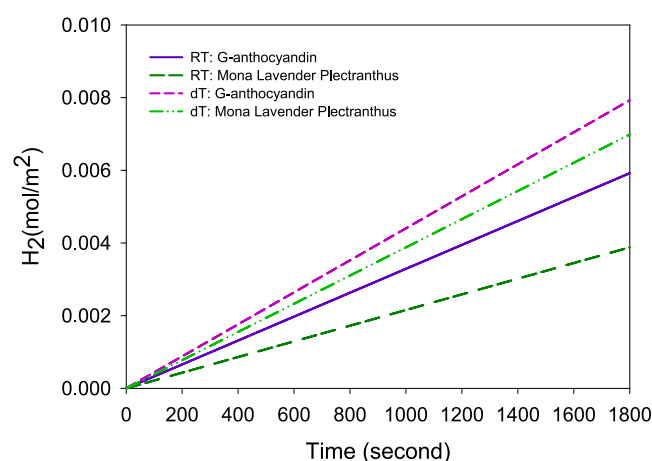
Figure 17. Hydrogen generation rate of water-splitting cell systems.

During water-splitting processing, WS$_2$ nanosheets with suitable energy level[35] displayed photocurrent densities as high as 4.5 A/m^2.[14] According to the energy level, our electrolyte was changed by the loaded photosensitizers. The conduction band of the WS$_2$ is −4.7 eV and the valence band is −5.9 eV with reference to the vacuum energy level.[13,15]

The water-splitting process is proposed in Figure 15. WS$_2$ was coated on the precleaned ITO glasses and settled in the electrolyte at pH 1 to fit the energy level of pigments. As the mechanism of water-splitting process in Figure 15 shows, the excited electrons were created by the natural halochromic pigments and WS$_2$ provided the supernumerary excited electrons to the system. The excited electrons followed the circuit to Pt cathodes and reduced the hydrogen ions into hydrogen gases.

The $J-V$ curve of the water splitting system is plotted in Figure 16. The current density of the G-anthocyanin-loaded electrolyte was much higher than MLP-loaded one, which is shown in the Figure 16a. A similar trend is also shown in Figure 16b, where the temperature difference was 40 °C.

The hydrogen generation rate is plotted in Figure 17. The rate is determined under the optimal applying parameters and the unit is set as mol m^2/s. The maximum hydrogen generation rate is demonstrated in G-anthocyanin-loaded electrolyte when the temperature difference is 40 °C. About 0.008 mol hydrogen gases is generated during a half hour.

From the energy level of WS$_2$ and natural halochromic pigments, the conduction band energy level of WS$_2$ was much higher than the occupied molecular orbital (HOMO) state of G-anthocyanin and MLP. Thus, the excited electrons of the WS$_2$ should be easily transported to the G-anthocyanin in the electrolyte for forming water-splitting processing by hopping phenomena.

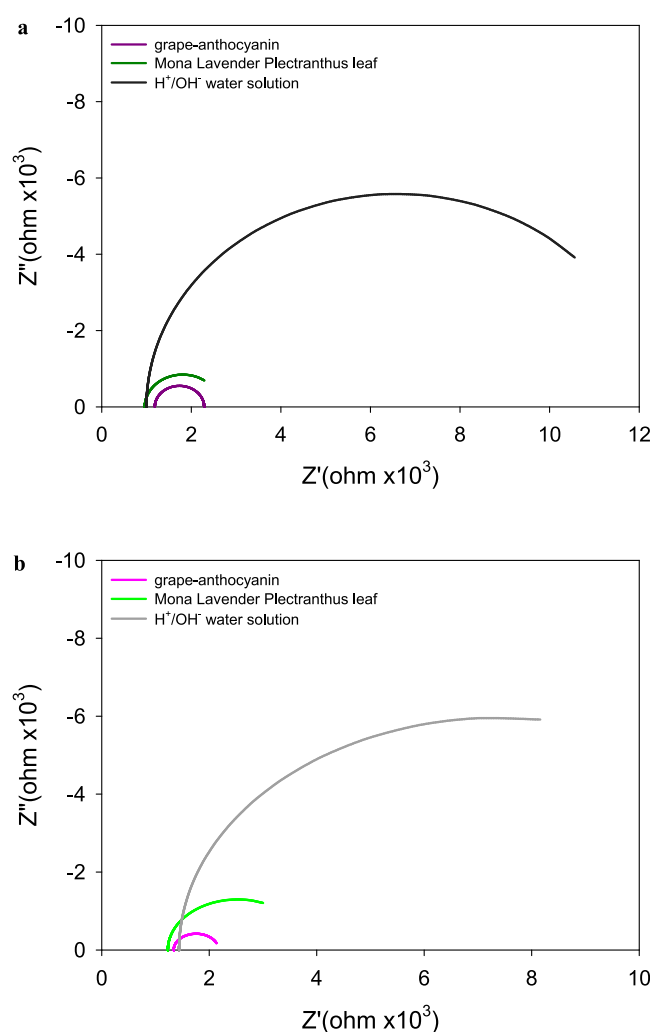In the water-splitting system, the excited electrons were generated from WS$_2$ and the halochromic pigments. The CH

Figure 18. Nyquist diagram of WS$_2$-based water splitting within halochromic pigments loaded electrolytes under AM 1.5G irradiation. (a) Electrolytes with temperature difference of 0 °C and (b) electrolytes with temperature difference of 40 °C.

Instrument provides the support current to inject electrons into electrolyte at pH 1 to generate hydrogen. As the CH Instrument provided the support current, the water splitting efficiency was raised and the working potential was reduced. The following details were listed in the Table 4, which shows the power of the water splitting was saved. In theoretical calculation, to generate 1 mol of hydrogen 237.4 KW/m^2 is needed. Furthermore, from the results of turnover frequency (TOF), the G-anthocyandin-loaded electrolytes under a 40 °C temperature difference demonstrated the highest electrocatalytic activity.

From WS$_2$-coated water-splitting cell and dissolution of G-anthocyanin in the electrolyte, 39.76% power (compared with the theoretical power of hydrogen generation) was saved to

Table 4. Detailed Result of Water-Splitting Cells Systems[a]

	$J_{\text{at 1.23 V}}$ (A/m^2)	J_{op} (A/m^2)	1.23 - E_{op} (V)	η	TOF[b] (μmol/sec·m^2)
RT: G-anthocyandin	1.407 ± 0.103	0.635 ± 0.094	0741 ± 0.051	39.76% ± 5%	3.290 ± 0.467
RT: Mona Lavender Plectranthus	1.225 ± 0.117	0.416 ± 0.083	0.808 ± 0.063	34.31% ± 2%	2.155 ± 0.430
dT: G-anthocyandin	1.806 ± 0.128	0.850 ± 0.105	0.614 ± 0.072	50.08% ± 3%	4.404 ± 0.544
dT: Mona Lavender Plectranthus	1.352 ± 0.092	0.749 ± 0.077	0.566 ± 0.058	53.98% ± 4%	3.881 ± 0.399

[a]Every result was tested with at least 10 samples. [b]TOF: turnover frequency which is determined under optimal operation applied voltages for H$_2$ evolution.

Table 5. Charge Dynamic Calculation[a]

	R_S (Ω m)	σ (S/m)	D (m^2/s)	μ (m^2/(V s))
RT: G-anthocyandin	1102 ± 92	0.91 ± 0.038	0.059 ± 0.007	1.42 ± 0.05 × 10^{19}
RT: Mona Lavender plectranthus	1692 ± 137	0.59 ± 0.023	0.038 ± 0.003	9.23 ± 0.17 × 10^{18}
dT: G-anthocyandin	835 ± 53	1.20 ± 0.046	0.078 ± 0.006	1.88 ± 0.02 × 10^{19}
dT: Mona Lavender plectranthus	2595 ± 183	0.39 ± 0.017	0.025 ± 0.002	6.02 ± 0.08 × 10^{18}

[a]Every result was tested with at least 10 samples.

generate 1 mol of hydrogen gases. As the temperature difference was created for increasing the efficiency, in MLP dissolved electrolyte coated with WS$_2$, about 54% energy was saved to generate 1 mol of hydrogen gases (compared with the theoretical power of hydrogen generation).

The charge mobility of the excited electrons was analyzed by electrochemical impedance spectroscopy (EIS). From Nyquist diagram of the WS$_2$ based water splitting within halochromic pigments loaded electrolytes under AM 1.5G irradiation (Figure 18), interface resistance of the one loaded with halochromic pigments was much lower than the electrolyte without any pigments loading. The charge mobility rose when the temperature difference was induced into the water splitting system to increase hydrogen generation efficiency (Table 5). WS$_2$-coated water-splitting cell in the electrolyte with G-anthocyanin demonstrated the highest charge mobility when the electrolytes were placed in an environment with a 40° temperature difference.

CONCLUSION

The system successfully combined waste heat within photo-electric conversion for power generation and hydrogen evolution. The liquid-type energy-yielding thermocells were achieved in narrow temperature difference. Waste heat, difficult to recycle, was successfully utilized in the power regeneration. Electron transfer ability of the solar cell was raised by loading natural halochromic pigments. Furthermore, electron diffusion coefficient achieved five times higher than the cells without halochromic pigments. The highest power 0.116 W/m^2 and the highest current density 0.29 A/m^2 were generated by Mona Lavender Plectranthus loaded liquid-type energy-yielding thermocells. Temperature difference of 40 degree kept the desired cell working stably. The solar cells were also converted into the water-splitting hydrogen-evolution cell with efficiency of more than 50%, which means the WS$_2$-based water-splitting cells in the thermocell dual system is able to save half of the theoretical input power for hydrogen evolution. In comparison with the literature,[27] our thermal cell demonstrated higher thermal sensitivity and the design in this study also demonstrated higher application ability in normal environment conditions.

AUTHOR INFORMATION

Corresponding Author

*Email: yhsu@mail.ncku.edu.tw.

ORCID

Yi-Sheng Lai: 0000-0001-5897-8763
Fei Pan: 0000-0002-9801-5619
Qun Ren: 0000-0003-0627-761X

Notes

The authors declare no competing financial interest.

REFERENCES

(1) Lamnatou, C.; Chemisana, D. Photovoltaic/thermal (PVT) systems: A review with emphasis on environmental issues. *Renewable Energy* **2017**, *105*, 270−287.

(2) Lv, H. J.; Geletii, Y. V.; Zhao, C. C.; Vickers, J. W.; Zhu, G. B.; Luo, Z.; Song, J.; Lian, T. Q.; Musaev, D. G.; Hill, C. L. Polyoxometalate water oxidation catalysts and the production of green fuel. *Chem. Soc. Rev.* **2012**, *41* (22), 7572−7589.

(3) Maeda, K. Z-Scheme Water Splitting Using Two Different Semiconductor Photocatalysts. *ACS Catal.* **2013**, *3* (7), 1486−1503.

(4) Vassel, S.; Vassel, N. A hybrid of thermogalvanic and concentration galvanic cells as an effective device for converting low-potential heat energy into electricity. *Int. J. Heat Mass Transfer* **2017**, *108*, 2333−2337.

(5) Kang, S. H.; Jeong, M. J.; Eom, Y. K.; Choi, I. T.; Kwon, S. M.; Yoo, Y.; Kim, J.; Kwon, J.; Park, J. H.; Kim, H. K. Porphyrin Sensitizers with Donor Structural Engineering for Superior Performance Dye-Sensitized Solar Cells and Tandem Solar Cells for Water Splitting Applications. *Adv. Energy. Mater.* **2017**, *7* (7), 1602117.

(6) Ning, Z. J.; Gong, X. W.; Comin, R.; Walters, G.; Fan, F. J.; Voznyy, O.; Yassitepe, E.; Buin, A.; Hoogland, S.; Sargent, E. H. Quantum-dot-in-perovskite solids. *Nature* **2015**, *523* (7560), 324−328.

(7) Yu, P. L.; Norinaga, K.; Watanabe, H.; Kitagawa, T. Prediction of hot coke oven gas reforming by LES coupled with the extended flamelet/progress variable approach. *Fuel* **2018**, *231*, 234−243.

(8) Sygletou, M.; Petridis, C.; Kymakis, E.; Stratakis, E. Advanced Photonic Processes for Photovoltaic and Energy Storage Systems. *Adv. Mater.* **2017**, *29* (39), 1700335.

(9) Yang, G.; Mo, J.; Kang, Z.; Dohrmann, Y.; List, F. A.; Green, J. B.; Babu, S. S.; Zhang, F.-Y. Fully printed and integrated electrolyzer cells with additive manufacturing for high-efficiency water splitting. *Appl. Energy* **2018**, *215*, 202−210.

(10) Afzal, A. M.; Khan, M. F.; Nazir, G.; Dastgeer, G.; Aftab, S.; Akhtar, I.; Seo, Y.; Eom, J. Gate Modulation of the Spin-orbit Interaction in Bilayer Graphene Encapsulated by WS$_2$ films. *Sci. Rep.* **2018**, *8* (1), 3412.

(11) Lai, Y.-S.; Su, Y. H.; Lin, M. I. Photochemical water splitting performance of fluorescein, rhodamine B, and chlorophyll-Cu supported on ZrO$_2$ nanoparticles layer anode. *Dyes Pigm.* **2014**, *103*, 76−81.

(12) Lai, Y.-S.; Pan, F.; Su, Y.-H. Firefly-like Water Splitting Cells Based on FRET Phenomena with Ultrahigh Performance over 12%. *ACS Appl. Mater. Interfaces* **2018**, *10* (5), 5007−5013.

(13) Liu, Q.; Liu, Q.; Kong, X. Anion Engineering on Free-Standing Two-Dimensional MoS2 Nanosheets toward Hydrogen Evolution. *Inorg. Chem.* **2017**, *56* (19), 11462−11465.

(14) Pesci, F. M.; Sokolikova, M. S.; Grotta, C.; Sherrell, P. C.; Reale, F.; Sharda, K.; Ni, N.; Palczynski, P.; Mattevi, C. MoS$_2$/WS$_2$

Heterojunction for Photoelectrochemical Water Oxidation. *ACS Catal.* **2017**, *7* (8), 4990−4998.

(15) Luo, Y.; Li, X.; Cai, X.; Zou, X.; Kang, F.; Cheng, H.-M.; Liu, B. Two-Dimensional MoS$_2$ Confined Co(OH)2 Electrocatalysts for Hydrogen Evolution in Alkaline Electrolytes. *ACS Nano* **2018**, *12* (5), 4565−4573.

(16) Lai, Y.-S.; Lu, H.-H.; Su, Y.-H. High-Efficiency Water-Splitting Solar Cells with Low Diffusion Resistance Corresponding to Halochromic Pigments Interfacing with ZrO$_2$. *ACS Sustainable Chem. Eng.* **2017**, *5* (9), 7716−7722.

(17) Zinatloo-Ajabshir, S.; Salavati-Niasari, M. Facile route to synthesize zirconium dioxide (ZrO2) nanostructures: Structural, optical and photocatalytic studies. *J. Mol. Liq.* **2016**, *216*, 545−551.

(18) Pan, L.; Xu, H.; Sun, Y.; Zhao, J.; Li, Y. Preparation of Three-Dimensional Photonic Crystals of Zirconia by Electrodeposition in a Colloidal Crystals Template. *Crystals* **2016**, *6* (7), 76.

(19) Plata, J. J.; Márquez, A. M.; Sanz, J. F. Electron Mobility via Polaron Hopping in Bulk Ceria: A First-Principles Study. *J. Phys. Chem. C* **2013**, *117* (28), 14502−14509.

(20) Sutton, J. E.; Beste, A.; Overbury, S. H. Origins and implications of the ordering of oxygen vacancies and localized electrons on partially reducedCeO$_2$(111). *Phys. Rev. B: Condens. Matter Mater. Phys.* **2015**, *92* (14), No. 144105.

(21) Zhang, J. Q.; Li, L.; Xiao, Z. X.; Liu, D.; Wang, S.; Zhang, J. J.; Hao, Y. T.; Zhang, W. Z. Hollow Sphere TiO$_2$-ZrO$_2$ Prepared by Self-Assembly with Polystyrene Colloidal Template for Both Photocatalytic Degradation and H$_2$ Evolution from Water Splitting. *ACS Sustainable Chem. Eng.* **2016**, *4* (4), 2037−2046.

(22) Zou, J.; Zeng, H.; Wang, Y.; Li, Y. H$^+$ Intercalation into Molybdenum Oxide Nanosheets Under AFM Tip Bias. *Phys. Status Solidi RRL* **2018**, *12*, 1700439.

(23) Wang, Y.; Carey, B. J.; Zhang, W.; Chrimes, A. F.; Chen, L.; Kalantar-zadeh, K.; Ou, J. Z.; Daeneke, T. Intercalated 2D MoS$_2$ Utilizing a Simulated Sun Assisted Process: Reducing the HER Overpotential. *J. Phys. Chem. C* **2016**, *120* (4), 2447−2455.

(24) Liu, X.; Gao, S.; Yang, P.; Wang, B.; Ou, J. Z.; Liu, Z.; Wang, Y. Synergetic coupling of Pd nanoparticles and amorphous MoS toward highly efficient electrocatalytic hydrogen evolution reactions. *Appl. Mater. Today.* **2018**, *13*, 158−165.

(25) Gu, W.; Yan, Y.; Zhang, C.; Ding, C.; Xian, Y. One-Step Synthesis of Water-Soluble MoS$_2$ Quantum Dots via a Hydrothermal Method as a Fluorescent Probe for Hyaluronidase Detection. *ACS Appl. Mater. Interfaces* **2016**, *8* (18), 11272−11279.

(26) Zhang, X.; Lai, Z.; Liu, Z.; Tan, C.; Huang, Y.; Li, B.; Zhao, M.; Xie, L.; Huang, W.; Zhang, H. A facile and universal top-down method for preparation of monodisperse transition-metal dichalcogenide nanodots. *Angew. Chem., Int. Ed.* **2015**, *54* (18), 5425−5428.

(27) Zhang, L.; Kim, T.; Li, N.; Kang, T. J.; Chen, J.; Pringle, J. M.; Zhang, M.; Kazim, A. H.; Fang, S. L.; Haines, C.; Al-Masri, D.; Cola, B. A.; Razal, J. M.; Di, J. T.; Beirne, S.; MacFarlane, D. R.; Gonzalez-Martin, A.; Mathew, S.; Kim, Y. H.; Wallace, G.; Baughman, R. H. High Power Density Electrochemical Thermocells for Inexpensively Harvesting Low-Grade Thermal Energy. *Adv. Mater.* **2017**, *29* (12), 1605652.

(28) Wu, J.; Black, J. J.; Aldous, L. Thermoelectrochemistry using conventional and novel gelled electrolytes in heat-to-current thermocells. *Electrochim. Acta* **2017**, *225*, 482−492.

(29) Daeneke, T.; Uemura, Y.; Duffy, N. W.; Mozer, A. J.; Koumura, N.; Bach, U.; Spiccia, L. Aqueous dye-sensitized solar cell electrolytes based on the ferricyanide-ferrocyanide redox couple. *Adv. Mater.* **2012**, *24* (9), 1222−5.

(30) Su, T.; Shao, Q.; Qin, Z.; Guo, Z.; Wu, Z. Role of Interfaces in Two-Dimensional Photocatalyst for Water Splitting. *ACS Catal.* **2018**, *8* (3), 2253−2276.

(31) Chen, T.-Y.; Chang, Y.-H.; Hsu, C.-L.; Wei, K.-H.; Chiang, C.-Y.; Li, L.-J. Comparative study on MoS$_2$ and WS$_2$ for electrocatalytic water splitting. *Int. J. Hydrogen Energy* **2013**, *38* (28), 12302−12309.

(32) Roldán, R.; Silva-Guillén, J. A.; López-Sancho, M. P.; Guinea, F.; Cappelluti, E.; Ordejón, P. Electronic properties of single-layer and multilayer transition metal dichalcogenidesMX$_2$(M= Mo, W and X= S, Se). *Ann. Phys.* **2014**, *526* (9−10), 347−357.

(33) Berkdemir, A.; Gutiérrez, H. R.; Botello-Méndez, A. R.; Perea-López, N.; Elías, A. L.; Chia, C.-I.; Wang, B.; Crespi, V. H.; López-Urías, F.; Charlier, J.-C.; Terrones, H.; Terrones, M. Identification of individual and few layers of WS$_2$ using Raman Spectroscopy. *Sci. Rep.* **2013**, *3*, 1755.

(34) Hou, J.; Zhao, G.; Wu, Y.; He, J.; Hao, X. Femtosecond solid-state laser based on tungsten disulfide saturable absorber. *Opt. Express* **2015**, *23* (21), 27292−27298.

(35) Mao, X.; Xu, Y.; Xue, Q.; Wang, W.; Gao, D. Ferromagnetism in exfoliated tungsten disulfide nanosheets. *Nanoscale Res. Lett.* **2013**, *8* (1), 430.